ACCSCIENCE PUBLISHING

Materials Science in Additive Manufacturing

ORIGINAL RESEARCH ARTICLE

Machine learning and RSM-based optimization of mechanical properties in MXene-reinforced PLA composites for additive manufacturing applications

Sundarasetty Harishbabu[1], P. S. Rama Sreekanth[1], Alagesan Praveen Kumar[2], Santosh Kumar Sahu[1]*, Nitesh Dhar Badgayan[3], Mohan Kumar Siddalingaiah[4], Razaullah Hafiz Ullah[5,6], and Mohammed Aman[5]*

[1]School of Mechanical Engineering, VIT-AP University, Amaravati, Andhra Pradesh, India

[2]Department of Mechanical Engineering, Easwari Engineering College, Chennai, Tamil Nadu, India

[3]Ernst and Young Services Private Limited, Gurgaon, Haryana, India

[4]Department of Mechanical Engineering, Amrita School of Engineering, Amrita Vishwa Vidyapeetham, Bengaluru, Karnataka, India

[5]Department of Industrial Engineering, College of Engineering, University of Business and Technology, Jeddah, Saudi Arabia

[6]Department of Industrial Engineering, Faculty of Architecture and Engineering, Bahçeşehir Cyprus University, Nicosia, Northern Cyprus, Turkiye

***Corresponding authors:**
Santosh Kumar Sahu (santoshkumar.sahu@vitap.ac.in);
Mohammed Aman (m.aman@ubt.edu.sa)

Citation: Harishbabu S, Sreekanth PSR, Kumar AP, *et al*. Machine learning and RSM-based optimization of mechanical properties in MXene-reinforced PLA composites for additive manufacturing applications. *Mater Sci Add Manuf*. doi: 10.36922/MSAM026350085

Received: August 28, 2026

Revised: October 1, 2026

Accepted: October 8, 2026

Published online: November 5, 2026

Copyright: © 2026 Author(s). This is an Open-Access article distributed under the terms of the Creative Commons Attribution License, permitting distribution, and reproduction in any medium, provided the original work is properly cited.

Publisher's Note: AccScience Publishing remains neutral with regard to jurisdictional claims in published maps and institutional affiliations.

Abstract

The mechanical properties of fused deposition modeling (FDM)-printed polymer composites depend on both material composition and printing parameters, necessitating systematic optimization and reliable predictive modeling. This study investigates the effects of material composition and process parameters on the mechanical properties of FDM-processed, MXene-reinforced polylactic acid (PLA) composites using response surface methodology (RSM) and machine learning (ML). Thirty-one experimental runs were conducted by varying MXene content (0–0.05 wt.%), outer shells (2–4), orientation angle (0°–90°), nozzle temperature (190 °C–210 °C), and printing speed (20–60 mm/s). Tensile strength, Young's modulus, and Vickers hardness ranged from 1.11–27.00 MPa, 326–2,969 MPa, and 44.6–84.3 HV, respectively. Maximum tensile strength was obtained at 0.05 wt.% MXene and 0° orientation, whereas Young's modulus was highest at 0.025 wt.% MXene with four outer shells. The highest hardness of 84.3 HV was obtained at 0.025 wt.% MXene and 45° orientations, with three outer shells, a nozzle temperature of 200 °C, and a printing speed of 60 mm/s. ANOVA indicated that the developed regression models reported R^2 values above 0.90 and insignificant lack-of-fit tests ($p > 0.05$). MXene content affected tensile strength and hardness, while outer shells and nozzle temperature significantly influenced stiffness. Among the evaluated ML models, LightGBM showed the highest model-fit R^2 values of 0.964, 0.965, and 0.935 for tensile strength, Young's modulus, and hardness, respectively. Evaluation using five additional experimentally tested conditions showed reasonable agreement between predicted and measured responses, with R^2 values of 0.846, 0.881, and 0.856 for tensile strength, Young's modulus, and hardness, respectively. SHAP and Pearson analyses further identified the dominant process parameters. These results demonstrate the

potential of combining RSM and ML for data-driven analysis and optimization of FDM-processed PLA/MXene composites for potential applications in automotive components, sports equipment, and customized functional parts.

Keywords: MXene; Polylactic acid; Optimization; Machine learning; Tensile strength

1. Introduction

Fused deposition modeling (FDM), a 3D printing technique, has emerged as a transformative manufacturing process, enabling the fabrication of complex and customized components with minimal material waste and reduced production time. Its adoption has expanded across key sectors such as aerospace, healthcare, and automotive industries, mainly because of its design flexibility and process efficiency. Concurrently, the widespread use of polymeric materials has increased owing to their low cost, lightweight nature, and durability.[1,2] Among these, polylactic acid (PLA) has garnered considerable attention as a biodegradable aliphatic polyester derived from natural sources such as corn starch and sugarcane.[3,4] Owing to its biodegradability, biocompatibility, and ease of processing, PLA is increasingly considered a viable alternative to conventional petroleum-based polymers.[5,6] Despite these advantages, PLA has inherent limitations, including relatively low tensile strength and hardness, restricting its use in load-bearing and structural components. To overcome these shortcomings, researchers often use various nanofillers to reinforce virgin PLA. This approach has shown strong potential to enhance the mechanical and functional properties of PLA-based composites, broadening their applicability in advanced engineering applications.[7] Several studies have focused on improving PLA's mechanical performance by incorporating nanofillers. Kumar *et al.*[8] examined the influence of carbon nanofibers and found that the addition of 3 wt.% carbon nanofibers improved tensile strength and yield strength by 23.3% and 20%, respectively, although a reduction in elongation at break indicated decreased ductility. Bhattacharjee *et al.*[9] investigated the effect of nano-silica reinforcement (2, 4, and 6 wt.%) in PLA. The results revealed that at 6 wt.% nano-silica, tensile strength and Young's modulus increased by 19.6% and 43.2%, respectively. Triveni *et al.*[10] introduced nanocomposites by reinforcing graphene nanoplatelets synthesized from *Hibiscus rosa-sinensis* extract at 0.5 to 12.5 wt.% into PLA. It was found that tensile strength and modulus peaked at 68 MPa and 2,690 MPa at 6.5 wt.%, respectively. Thirugnanasambandam *et al.*[11] focused on synthesizing biodegradable PLA-based nanocomposites by reinforcing multiwalled carbon nanotubes (MWCNTs) at 0.5, 0.75, and 1 wt.% in PLA. The mechanical properties, such as tensile, compressive, and flexural strength, improved with the addition of MWCNTs. Yoon *et al.*[12] studied the mechanical properties of PLA composites reinforced with surface-modified halloysite nanotubes at 3, 5, 7, and 10 wt.%, including pure PLA. The results showed that small amounts of halloysite nanotubes (3–5 wt.%) enhanced the mechanical properties. Ab Ghani *et al.*[13] investigated the reinforcement of graphene nanoplatelets in PLA at 0.1, 0.3, 0.5, and 1 wt.% and found that tensile strength increased to 50.3 MPa at 0.3 wt.%. Ramachandran *et al.*[14] evaluated the effect of reinforcing PLA with nano-silica at 0, 2, 4, 6, and 8 wt.% and prepared filaments for additive manufacturing. The results show that adding 8 wt.% nano-silica yielded the highest tensile, flexural, and impact strengths, at 52 MPa each. Similarly, a hardness of 52 MPa was achieved. De Bortoli *et al.*[15] developed a PLA nanocomposite reinforced with functionalized carbon nanotubes (f-CNT), and the results showed that the addition of 0.5 wt.% f-CNT increased tensile strength from 29.4 ± 0.7 MPa to 41.6 ± 1.4 MPa (~41.5%) and improved storage modulus by ~43% at 37 °C.

Researchers have extensively studied methods to enhance the mechanical properties of PLA composites by reinforcing them with different nanofillers. However, PLA reinforced with MXene ($Ti_3C_2T_X$) remains understudied. MXene was chosen because of its high modulus (~500 GPa) and impressive tensile strength (~15.4 GPa), which are expected to enhance PLA's mechanical properties.[16,17] Many studies have used 3D printing to fabricate nanocomposite samples.[18,19] However, prior approaches lack systematic optimization and predictive capabilities that account for both material composition and printing parameters. The novelty of this research lies in its integration of optimization, comprising response surface experimental design and ANOVA, followed by the prediction of mechanical properties using a data-driven machine learning technique. This hybrid approach provides a comprehensive framework that not only optimizes the mechanical properties of PLA composites but also accurately predicts these properties using machine learning techniques. By bridging the gap between process-

parameter optimization and machine learning prediction, this research establishes a more efficient, predictive path to creating high-performance, biodegradable composites across industries such as biomedical, automotive, and aerospace.[20,21]

2. Materials and methods

2.1. Materials

Polylactic acid with a melt flow index of 2–4 g/10 min, with a specific gravity of 1.30–1.35 g/cm^3 in the form of granules, was obtained from Deltora Biopolymer Pvt. Ltd., India. MXene ($Ti_3C_2T_X$) with a density of 3.8 g/cm^3 in the form of flake-like morphology with an average particle size of 50–60 nm, having a purity of >99 %, was supplied by Nano Research Element, India. The supplied MXene was examined using scanning electron microscopy (Figure 1a), confirming flake-like morphology. The particle size distribution (Figure 1b) indicates an average particle size of 50–60 nm.

2.2. Experimental design

Statistical analysis is one of the systematic investigation techniques commonly used to identify the relationship between input parameters, such as printing parameters (e.g., number of outer shells [S], orientation angle [O], nozzle temperature [N], printing speed [P], along with composition [C] in wt.%, varying at three levels as shown in Table 1) and mechanical properties (e.g., tensile strength, Young's modulus, and hardness) obtained from the experiments for PLA/MXene composites. To analyze the relationship between input parameters and their levels, the current experiments were performed using an I-optimal design in response surface methodology (RSM) with Design-Expert 13 software (Stat-Ease, Inc., United States of America [USA]).[22-24]

2.3. Sample fabrication

The PLA/MXene composite samples were fabricated in three stages, as shown in Figure 2. Figure 2a illustrates the initial stage, in which MXene was incorporated into PLA at 0, 0.025, and 0.05 wt.% to obtain different composite compositions. MXene content was varied from 0 to 0.05 wt.% (nominal concentration), with the low-filler range selected to investigate the reinforcing effect of MXene while minimizing the potential for filler agglomeration.[25,26] MXene was weighed and dispersed in ethanol at a 20:1 weight ratio to ensure uniform distribution and prevent particle agglomeration. Sonication was performed for 30 min at 40 kHz. The solution was mixed with the PLA granules, continuously stirred on a hot plate, and dried until the solvent completely evaporated, yielding a homogeneous composite mixture, which was then vacuum-dried at 70 °C for 24 h to remove moisture. In the intermediate stage, the dried composite mixtures were processed through a twin-screw extruder operated with the barrel temperature ranging from 180 °C to 210 °C, with a die diameter of 2 mm at a speed of 15–30 rpm to extrude the filament diameter of 1.75 ± 0.05 mm by cooling the molten composite by passing it through the cold-water bath (Figure 2b). The obtained filament was collected and stored in an airtight container to avoid moisture absorption.[27,28] Figure 2c presents the final stage of sample fabrication; the extruded filaments were used to fabricate the test samples using an FDM Flash Forge printer (FlashForge Dreamer, Reddx Technologies Pvt Ltd., Chennai, India) with a 0.4 mm nozzle diameter, varying the printing parameters as per the design of experiment mentioned in Table 2.

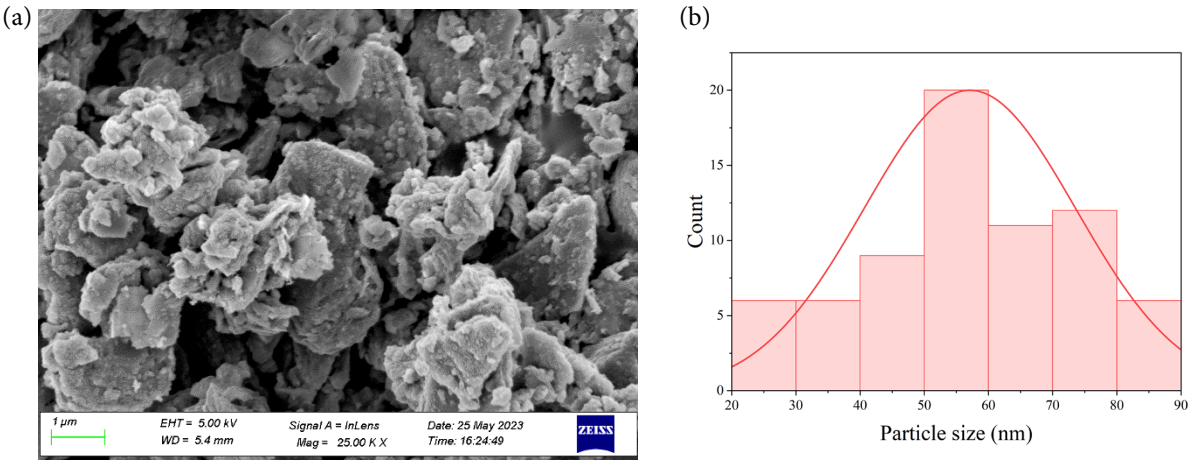


Figure 1. Characterization of MXene. (a) Morphology obtained using scanning electron microscopy. Scale bar: 1 µm; magnification: 25,000×. (b) Particle size distribution.

Table 1. Factors and levels for experimental design

Levels	Composition (C; wt.%)	No. of outer shells (S)	Orientation angle (O; °)	Nozzle temperature (N; °C)	Printing speed (P; mm/s)
Minimum	Pure PLA	2	Horizontal (0)	190	20
Maximum	0.05	4	Vertical (90)	210	60
Mean	0.025	3	Inclined (45)	200	40

Abbreviation: PLA: Polylactic acid.

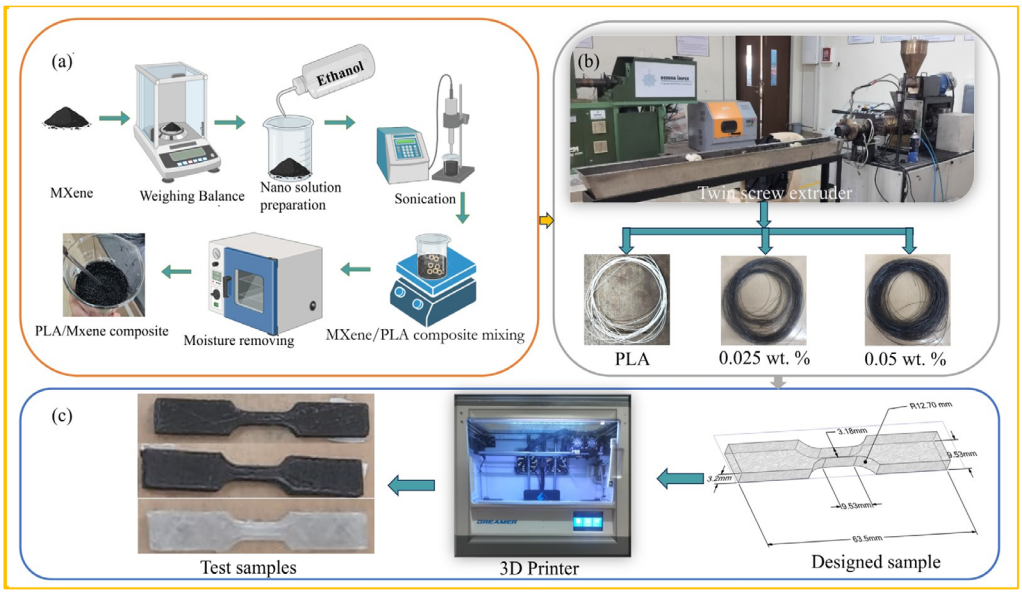


Figure 2. Fabrication steps. (a) Composition preparation. (b) Filament extrusion. (c) Sample printing.
Abbreviation: PLA: Polylactic acid.

The samples were fabricated according to the predefined geometry per ASTM D638, with a layer height of 0.18 mm, an infill density of 100%, a specimen orientation angle, and a grid infill pattern.[29]

2.4. Mechanical analysis

2.4.1. Tensile testing

The tensile strength and Young's modulus of PLA/MXene composites were assessed using tensile testing. The 3D-printed dog-bone samples (ASTM D638) were subjected to uniaxial loading using a universal testing machine (H10KL, Tinius Olsen India Pvt. Ltd., India). The test was performed under a crosshead speed of 2 mm/min. Three specimens were tested for each experimental condition, and the average value was used for analysis at room temperature.[30,31]

2.4.2. Hardness

Micro Vickers hardness testing was performed to analyze the hardness of MXene/PLA composites using a Vickers hardness tester (MC-AT, Fine Spavy Associates & Engineers Pvt. Ltd., India) in accordance with ASTM E384. A load of 0.05 kg was applied for 10 s.[32] The diagonal length of the indentation produced using the indenter was measured to assess the hardness using **Equation 1**.[33] The indentation was repeated in three trials, and the average values were used for analysis.

$$H = 0.1896 \frac{F \sin \frac{\varnothing}{2}}{k^2} \quad (1)$$

where F, $\varnothing$, and k are the load in N, indenter angle, and average length of the two diagonals, respectively.

2.5. Statistical analysis

Statistical analysis was performed using Design-Expert 13 (Stat-Ease, Inc., USA) to assess the model significance and the relationship between the input variables and the experimentally obtained responses using ANOVA at a 95% confidence level. The significance of the developed model was assessed using the coefficient of determination (R^2), the adjusted coefficient of determination (adj. R^2), and the predicted coefficient of determination (pred. R^2). Additionally, a lack-of-fit test was performed to analyze whether the model is acceptable.[34,35]

2.6. Machine learning

Machine learning is one of the most advanced data-driven techniques used to predict and analyze relationships among responses such as tensile strength, Young's modulus, and hardness of MXene/PLA composites, as printing parameters, including composition, vary. In this study, 31 experimentally obtained observations were used to train the models, and five newly generated and experimentally tested data points were used to validate the trained models independently. The models were trained using Python code on the Google Colab cloud platform. To evaluate the models' performance, several error metrics, including R^2, mean absolute error (MAE), mean squared error (MSE), and root mean square error (RMSE), were calculated using **Equations 2–5**.[36,37] In addition, visualization tools such as confusion matrices, Taylor diagrams, and SHapley Additive exPlanations (SHAP)-like interpretation techniques were employed to analyze the contribution of input parameters to response prediction and to provide a comprehensive evaluation of model interpretability.[38]

$$R^2 = 1 - \frac{\sum_{a=1}^{h}(A_a - \overset{\phi}{A}_a)^2}{\sum_{a=1}^{h}(A_a - \overset{\phi}{A})^2} \tag{2}$$

$$MAE = \frac{1}{h}\sum_{a=1}^{h}\left|A_a - \overset{\phi}{A}_a\right| \tag{3}$$

$$MSE = \frac{1}{h}\sum_{a=1}^{h}(A_a - \overset{\phi}{A}_a)^2 \tag{4}$$

$$RMSE = \sqrt{MSE} \tag{5}$$

where h, A_a, $\overset{\phi}{A}$, and $\overset{\phi}{A}_a$ are the total number of observations (experimental runs), actual (experimental) value, mean of the actual values, and predicted value corresponding to the a^{th} observation, respectively.

2.6.1. Multiple linear regression

Multiple linear regression (MLR) is the most widely used machine learning model in composites to quantify the relationship between input parameters, such as printing parameters including composition, and corresponding responses, such as tensile strength, Young's modulus, and hardness. The method estimates regression coefficients while accounting for the other input variables. The mathematical relationship between input variables and responses is expressed in **Equation 6**.[39]

$$R = \partial_0 + \partial_1 C + \partial_2 S + \partial_3 O + \partial_4 N + \partial_5 P + \varepsilon \tag{6}$$

where R represents the response variables, ∂_0 is the intercept, ∂_1, ∂_2, ..., ∂_5 are regression coefficients, and ε is the random error term. *C*, *S*, *O*, *N*, and *P* denote the composition and printing parameters.

2.6.2. Adaptive boosting

Adaptive boosting (AdaBoost) is an ensemble machine learning method that sequentially fits weak learners, with greater emphasis placed on observations associated with larger prediction errors in preceding iterations. The weighted combination of these learners produces the final regression prediction. In this study, AdaBoost is used to analyze the relationship between 3D printing input parameters, including composition, and the responses of MXene/PLA composites. This method sequentially trains the learning models, typically decision tree models. Each model focuses on samples that were incorrectly predicted previously. This process improves model efficiency by reducing the model error. The prediction is obtained by integrating the weighted outputs of all individual learning models. The mathematical expression for the prediction is given in **Equations 7 and 8**.[40]

$$F(R) = \sum_{a=1}^{h} W_a L_a(R) \tag{7}$$

$$W_a = \frac{1}{2} ln\left(\frac{1-\varepsilon_a}{\varepsilon_a}\right) \tag{8}$$

where $F(R)$, $W_a, L_a(R)$, and ε_a represent the final prediction, the weight assigned to the a^{th} learner, the prediction assigned to the a^{th} learner, and the error rate at the a^{th} learner, respectively.

2.6.3. Light gradient boosting machine

Light gradient boosting machine (LightGBM) is an advanced, highly efficient ensemble machine learning method, most commonly used for regression due to its accuracy. This model successively reduces prediction errors,

similar to gradient boosting. In this study, LightGBM was used to analyze the relationship between input parameters, such as composition and printing parameters, and the responses of MXene/PLA composites. This method employs a leaf-wise tree-growth strategy with constraints, enhancing model accuracy while reducing computational time. The model predicts responses by iteratively adding weak functions to minimize a specified loss. The mathematical relationship between input parameters and output responses is presented in **Equations 9 and 10**.[41,42]

$$F(X) = \sum_{a=1}^{h} f_a(X) \quad (9)$$

where $F(X)$, $f_a(X)$, $X(C,S,O,N,P)$, and h represent the final predicted response, the decision tree for the a[th] order, input parameters, and the total number of trees, respectively.

The objective function for each iteration is:

$$L_f = \sum_{j=1}^{k} \ell\left(R_j, \overset{\phi}{R}_j\right) + \sum_{a=1}^{h} \partial(f_a) \quad (10)$$

where $\ell\left(R_j, \overset{\phi}{R}_j\right)$, and $\partial(f_a)$ are the loss function and the regularization term that controls model complexity, respectively.

2.7. Experimental validation

For experimental validation, five additional validation data points were generated by varying the process parameters within an extended range of the original design space. Composition values were randomly selected from the experimentally investigated levels, whereas the number of shells, orientation angle, nozzle temperature, and printing speed were randomly generated within a range beyond their original minimum and maximum values. The selected validation data points are presented in Table 2. These conditions were supplied to the trained MLR, AdaBoost, and LightGBM models, and the resulting predictions were subsequently compared with experimentally measured responses.

3. Results and discussion

3.1. Design of experiments

Table 3 presents the experimental design with 31 randomized runs, employed to minimize the number of experiments. The design encoded a coordinate-exchange algorithm implemented in Design-Expert software. A reduced polynomial regression model was developed using significant linear, quadratic, and interaction terms selected based on ANOVA. The final model was retained with 14 degrees of freedom, while statistically insignificant terms were excluded to improve model parsimony. Therefore, the selected 31 runs provided sufficient experimental points to estimate these coefficients while maintaining adequate residual degrees of freedom for statistical validation and error estimation.

3.2. Mechanical analysis

3.2.1. Tensile testing

Figure 3 illustrates the experimental results for the 31 printed samples under varying printing parameters, including composition. In Figure 3a, tensile strength ranged from 1.11 to 27.0 MPa, showing significant variation due to changes in composition (0–0.05 wt.%) and printing parameters, such as the number of outer shells, raster orientation, nozzle temperature, and printing speed. The samples A9, A12, and A24 exhibited the highest tensile strength values of 27.0, 26.6, and 25.4 MPa, respectively, indicating superior load-bearing capacity under optimized conditions, particularly at 0° orientation and higher filler content (0.05 wt.%). Similarly, samples A8, A26,

Table 2. Experimental validation data points and corresponding process parameters

Composition (C; Wt.%)	No. of outer shells (S)	Orientation angle (O; °)	Nozzle temperature (N; °C)	Printing speed (P; mm/s)
0.05	2	32	193	36
0.025	4	64	210	52
0.025	3	16	191	41
Pure PLA	2	46	194	47
Pure PLA	3	23	210	25

Abbreviation: PLA: Polylactic acid.

and A21 reported 1.11, 7.67, and 10.1 MPa, respectively, indicating poor interlayer adhesion and unfavorable parameter combinations, such as 90° orientations, low shell numbers, and pure PLA composition. Young's moduli ranged from 326.40 MPa to 2,969.46 MPa (Figure 3b). The highest modulus was observed in A15, followed by A22 (2,082.29 MPa) and A27 (1,572.22 MPa), indicating that shell number and nozzle temperature significantly affect stiffness. Notably, the trends in tensile strength and Young's modulus do not perfectly align. For example, A15 exhibited the highest stiffness but not the highest tensile strength, indicating a nonlinear relationship between strength and stiffness. The ANOVA results indicate that composition is the dominant effect on tensile strength, while several interaction and nonlinear terms also contribute to the response.

3.2.2. Hardness

Figure 4 illustrates the hardness of MXene/PLA composites by varying 3D printing parameters and composition. The hardness of the composites ranged from 44.63 (A29) to 84.28 HV (A19), with higher hardness generally associated with moderate filler content (0.025 wt.%) and 45° orientations, suggesting improved resistance to localized deformation due to better filler dispersion and interfacial bonding. Similarly, A16 and A13 also showed higher hardness, with values of 81.68 and 80.25 HV, respectively. In contrast, the lowest hardness was reported in A29, corresponding to pure PLA. The ANOVA results reveal that composition, orientation angle, and printing speed significantly influenced hardness, whereas outer-shell number and nozzle temperature were not statistically significant at the 95% confidence level.

3.3. Statistical analysis

3.3.1. Analysis of variance

The ANOVA results presented in Table 4 confirm that the developed regression models were statistically significant, with *F*-values of 24.04, 15.18, and 10.44 for tensile strength, Young's modulus, and hardness, respectively ($p < 0.0001$). For tensile strength, composition was the most effective parameter with a *p*-value less than 0.0001, while the remaining factors were insignificant with *p*-values greater than 0.05. Moreover, the integration of CS, N^2, ON^2, CSO, and C^2O^2 showed strong combined and nonlinear effects, with a *p*-value less than 0.05. For Young's modulus, the number of outer shells and nozzle temperature exhibited the strongest main effects, with *F*-values of 86.04 and 32.30, respectively, followed by orientation angle ($F = 7.07$) and printing speed ($F = 4.70$), all of which were also statistically significant at the 95% confidence level. Similarly, for hardness, the highest *F*-values and *p*-values < 0.05 for composition, orientation angle, printing speed, and interaction terms such as CSN, CSP, SP^2, and S^2O^2 indicate that these factors significantly affect hardness. The model's evaluations, such as $R^2 > 86\%$ and adj. $R^2 > 75\%$, confirm that the models were well fitted, while the pre. $R^2 > 0.7$ indicates good predictive capability of the models. Furthermore, for all responses, the lack-of-fit was insignificant with *p*-values greater than 0.05, indicating that the models are reliable for predicting the responses.

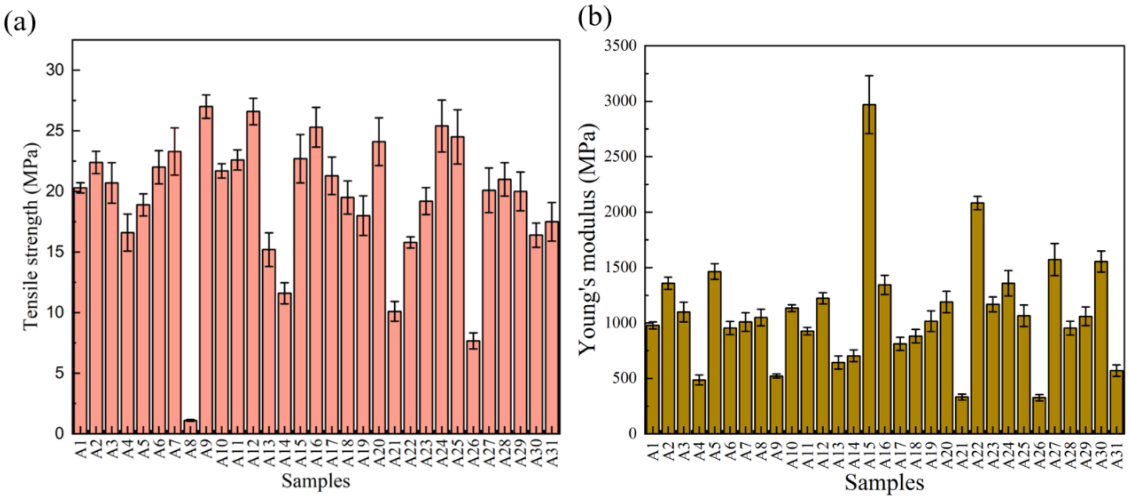


Figure 3. Experimentally obtained (a) tensile strength and (b) Young's modulus

Table 3. Experimental design and mechanical results obtained for PLA/MXene composites

Runs	Composition (C; wt.%)	No. of outer shells (S)	Orientation angle (O; °)	Nozzle temperature (N; °C)	Printing speed (P; mm/s)	Tensile strength (MPa)	Young's modulus (MPa)	Hardness (HV)
A1	0.05	2	90	210	40	20.3	978.39	50.875
A2	0.05	4	90	200	40	22.4	1,358.39	64.575
A3	0.025	3	90	200	20	20.7	1,099.66	60.675
A4	0.05	2	90	190	40	16.6	485.82	65.125
A5	0.05	3	45	210	20	18.9	1,464.29	72.175
A6	0	3	0	210	20	22.0	954.61	59.300
A7	0	4	0	190	60	23.3	1,009.61	66.225
A8	0	2	90	210	60	1.11	1,049.80	54.775
A9	0.05	2	0	200	20	27.0	521.61	61.150
A10	0.025	4	0	200	20	21.7	1,134.14	65.650
A11	0.025	3	45	200	60	22.6	926.99	72.900
A12	0.05	4	0	210	20	26.6	1,223.06	73.650
A13	0.025	2	45	210	40	15.2	643.75	80.250
A14	0	2	45	210	20	11.6	704.25	57.250
A15	0.025	4	0	210	40	22.7	2,969.46	65.975
A16	0.05	3	0	200	40	25.3	1,343.94	81.675
A17	0.05	2	45	210	60	21.3	812.59	57.700
A18	0.025	2	45	210	40	19.5	881.41	72.000
A19	0.025	3	45	200	60	18.0	1,016.37	84.275
A20	0.025	3	0	190	20	24.1	1,189.66	79.925
A21	0	4	90	190	60	10.1	332.17	61.550
A22	0	4	45	210	40	15.8	2,082.29	55.375
A23	0.05	4	45	190	20	19.2	1,168.16	69.125
A24	0.05	4	0	210	60	25.4	1,358.84	83.325
A25	0.05	3	0	200	40	24.5	1,065.20	69.200
A26	0	2	45	190	40	7.67	326.40	59.475
A27	0	2	0	210	60	20.1	1,572.22	67.875
A28	0.025	2	0	190	60	21.0	953.77	61.550
A29	0	2	0	200	20	20.0	1,060.11	44.625
A30	0.025	3	90	200	20	16.4	1,554.23	57.425
A31	0.025	3	45	200	60	17.5	570.72	75.375

Abbreviation: PLA: Polylactic acid.

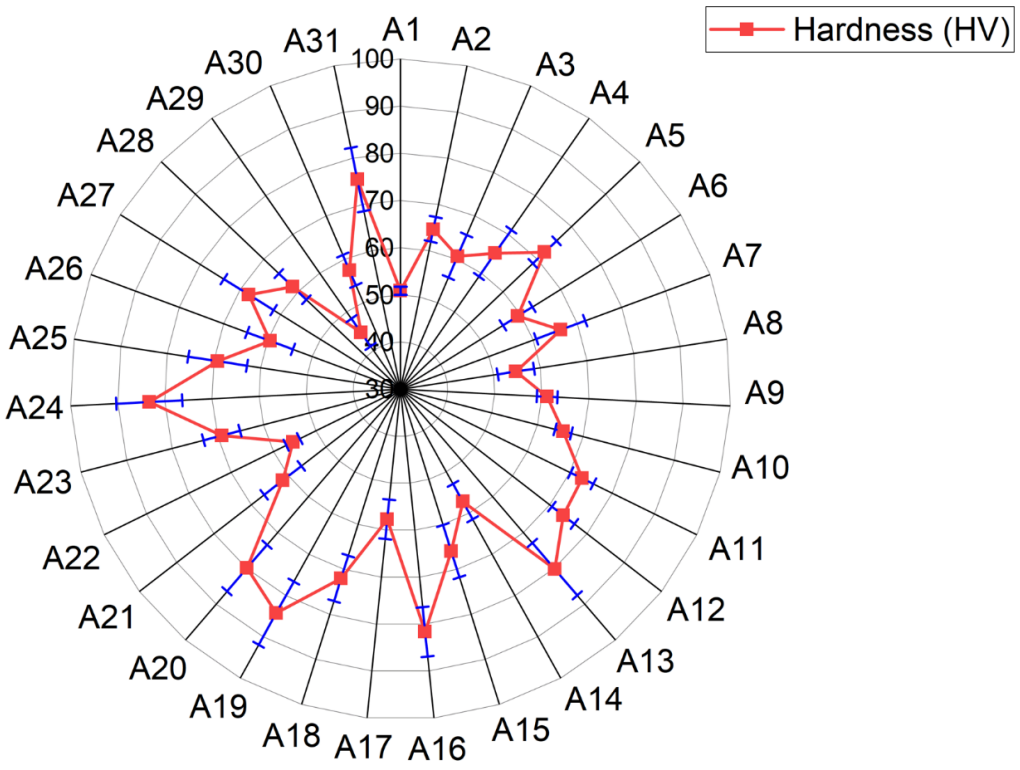


Figure 4. Experimentally obtained hardness

$$\text{Tensile strength (MPa)} = 19.67 + 3.56C + 0.4501S - 0.8761O + 0.1967N - 0.0005P - 2.66CS + 0.9629CO - 0.0031CN - 0.9797SN - 3.70N2 - 1.38CSO - 1.20S2P - 6.43ON2 + 1.75C2O2 \quad (11)$$

$$\text{Young's modulus (MPa)} = 966.79 + 70.85C + 1006.65S - 126.20O + 449.34N - 103.27P - 94.47ON - 366.62OP + 296.46N2 - 236.68COP - 376.44CNP - 572.24C2S - 483.39SP2 - 584.55NP2 - 85.97S2O2 \quad (12)$$

$$\text{Hardness (HV)} = 71.68 + 5.08C + 0.0483S - 4.22O - 1.17N + 6.45P - 4.90C2 + 2.95S2 - 1.18C2 + 6.75CSN + 4.23CSP - 2.33ONP + 4.75SP2 - 6.07N2P - 9.13S2O2 \quad (13)$$

The comparison between experimental and predicted responses based on statistical analysis using the regression model is illustrated in **Figure 5**. For tensile strength (**Figure 5a**), the predicted values were in close agreement with the experimental results, within ±5%. For example, A1, A2, and A9 exhibited experimental tensile strengths of 20.3, 22.4, and 27.0 MPa, respectively, with predicted values of 19.69, 21.47, and 26.96 MPa and with deviations of less than 5%, indicating high prediction accuracy. **Figure 5b** presents the deviation range of Young's modulus, approximately within ±10% for most runs. A1, A2, and A20, experimental values of 978.39, 1,358.39, and 1,189.66 MPa, respectively, yielded predictions of 1,022.39, 1,254.00, and 1,107.54 MPa. Although a few larger deviations were observed, the overall results suggest moderate variability. Similarly, hardness values exhibited acceptable agreement (Figure 5c), with most deviations within 10%, as illustrated by the experimental and predicted values of 50.88 and 52.33 HV (A1), 64.58 and 60.34 HV (A2), and 79.93 and 77.84 HV (A20), respectively. Most predictions fell within acceptable error margins, and the clustering of data points near the 45° reference line confirms that the model provides reliable and accurate predictions of mechanical properties.

The contour plots in Figure 6 present the influence of printing parameters on the tensile strength of various samples. The color variations ranged from 1.11 (blue at lower) to 27.0 MPa (red at higher). In Figure 6a, tensile strength increased from 10.0 to 27.0 MPa as the MXene composition increased from 0 to 0.05 wt.%, and the number of outer shells was optimized at 3. In Figure 6b,

Table 4. Analysis of variance for the target variables

Source	Tensile strength		Young's modulus		Hardness		df
	F-value	*p*-value	*F*-value	*p*-value	*F*-value	*p*-value	
Model	24.04	<0.0001	15.18	<0.0001	10.44	<0.0001	14
C	67.62	<0.0001	2.26	0.1521	21.87	0.0003	1
S	1.06	0.3190	86.04	<0.0001	0.0008	0.9772	1
O	1.03	0.3241	7.07	0.0172	17.00	0.0008	1
N	0.23	0.6400	32.30	<0.0001	1.04	0.3234	1
P	5.98×10^{-7}	0.9994	4.70	0.0455	9.00	0.0085	1
CS	26.44	<0.0001	1.92	0.1847	7.43	0.0150	1
CO	2.94	0.1059	36.05	<0.0001	0.71	0.4123	1
CN	0	0.9950	12.70	0.0026	0.10	0.7531	1
SN	4.21	0.0568	9.25	0.0078	18.69	0.0005	1
N^2	24.55	0.0001	28.68	<0.0001	6.65	0.0202	1
CSO	5.59	0.0310	22.97	0.0002	2.37	0.1432	1
S^2P	1.29	0.2723	24.12	0.0002	4.93	0.0411	1
ON^2	25.87	0.0001	28.02	<0.0001	4.46	0.0509	1
C^2O^2	5.96	0.0266	1.21	0.2876	4.84	0.0429	1
Residual							16
Lack of fit	0.1221	0.9981	0.4523	0.8733	0.2331	0.9793	11
Pure error							5
Cor. total							30
R^2	0.9546		0.9300		0.9013		
Adjusted R^2	0.9149		0.8687		0.8150		
Predicted R^2	0.8707		0.7003		0.7072		

Abbreviation: df: Degrees of freedom.

a 0.05 wt.% MXene composition yielded a maximum tensile strength of 27.0 MPa, whereas an orientation angle of 60° had a moderate effect. In Figure 6c, similarly, the tensile strength significantly improved with higher composition, combined with nozzle temperatures around 200 °C, yielding 27.0 MPa. In Figure 6d, the interaction between orientation angle and nozzle temperature showed nonlinear behavior. The results suggest that composition is the most influential factor, while other parameters interact to optimize performance.

Figure 7 shows the influence of printing parameters on Young's modulus. In Figure 7a, the Young's modulus increased from 1,049.00 to 2,969.00 MPa as composition increased from 0 to 0.025 wt.%, with an optimal number of outer shells around 4. In Figure 7b, the Young's modulus significantly improved with an increasing number of outer shells, reaching around 2,969.00 MPa, while the orientation angle of 60° showed moderate performance. In Figure 7c, moderate printing speeds of 40–60 mm/s and high shell numbers yielded Young's moduli above 2,000.00 MPa. Similarly, in Figure 7d, an increase in Young's modulus was observed at higher nozzle temperatures (200 °C–210 °C) and moderate printing speeds. The results suggest that the number of outer shells and nozzle temperature are the dominant factors, while composition and printing speed exhibit interactive effects on Young's modulus.

Figure 8 illustrates the influence of printing parameters on hardness for MXene/PLA composites, with values

ranging from 44.63 (blue) to 84.28 HV (red). In Figure 8a, the contour response shows that hardness varied nonlinearly with MXene composition, with the highest experimentally measured hardness of 84.28 HV occurring at 0.025 wt.% under the corresponding experimental process conditions. In Figure 8b, the orientation angle showed minimal effect on hardness, with negligible improvement observed at 60°, whereas the hardness of the MXene/PLA composite improved with increasing number of outer shells. In Figure 8c, hardness of 70.00 to 84.28 HV was achieved at printing speeds of 40–60 mm/s as the shell number increased. Similarly, in Figure 8d, at a nozzle temperature of 200 °C–210 °C, the highest hardness was observed at moderate printing speeds with a strong influence. The results show that composition and number of outer shells are the dominant factors, while orientation angle, printing speed, and nozzle temperature collectively influence hardness.

3.4. Machine learning

Figure 9 presents the performance of comparative parity plots using different machine learning models predicting responses such as tensile strength, Young's modulus, and hardness of MXene/PLA composites. The circular (green), triangular (yellow), and pentagonal (greenish-blue) points represent predicted values from MLR, AdaBoost, and LightGBM. The diagonal line represents the ideal line based on the proximity of data points; when predicted and experimental values match, the data points' proximity to this line indicates prediction accuracy. In Figure 9a, the predicted tensile strength was in strong agreement with experimental values for LightGBM, with deviations below 10%. AdaBoost exhibited moderate agreement, with most deviations between 10% and 18%, whereas MLR exhibited significantly larger deviations, up to 30%, as evidenced by tighter clustering along the diagonal. In Figure 9b, the predicted Young's modulus had strong agreement with experimental values for LightGBM, with deviations mostly below 10%. AdaBoost exhibited moderate deviation, with experimental values between 5% and 21%, whereas MLR exhibited significantly larger deviations, up to 45%. Similarly, for hardness (Figure 9c), LightGBM and AdaBoost showed the best alignment, with most predictions below 10%, whereas MLR exhibited

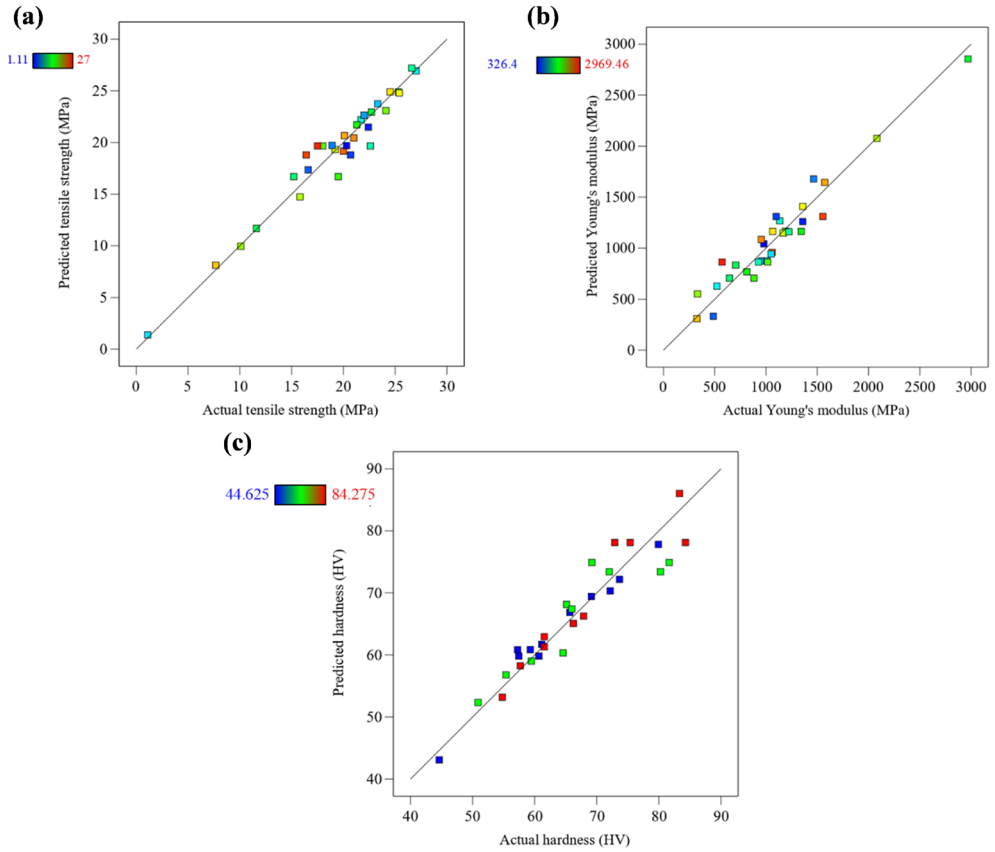


Figure 5. Experimental versus predicted values of (a) tensile strength, (b) Young's modulus, and (c) hardness for statistical analysis

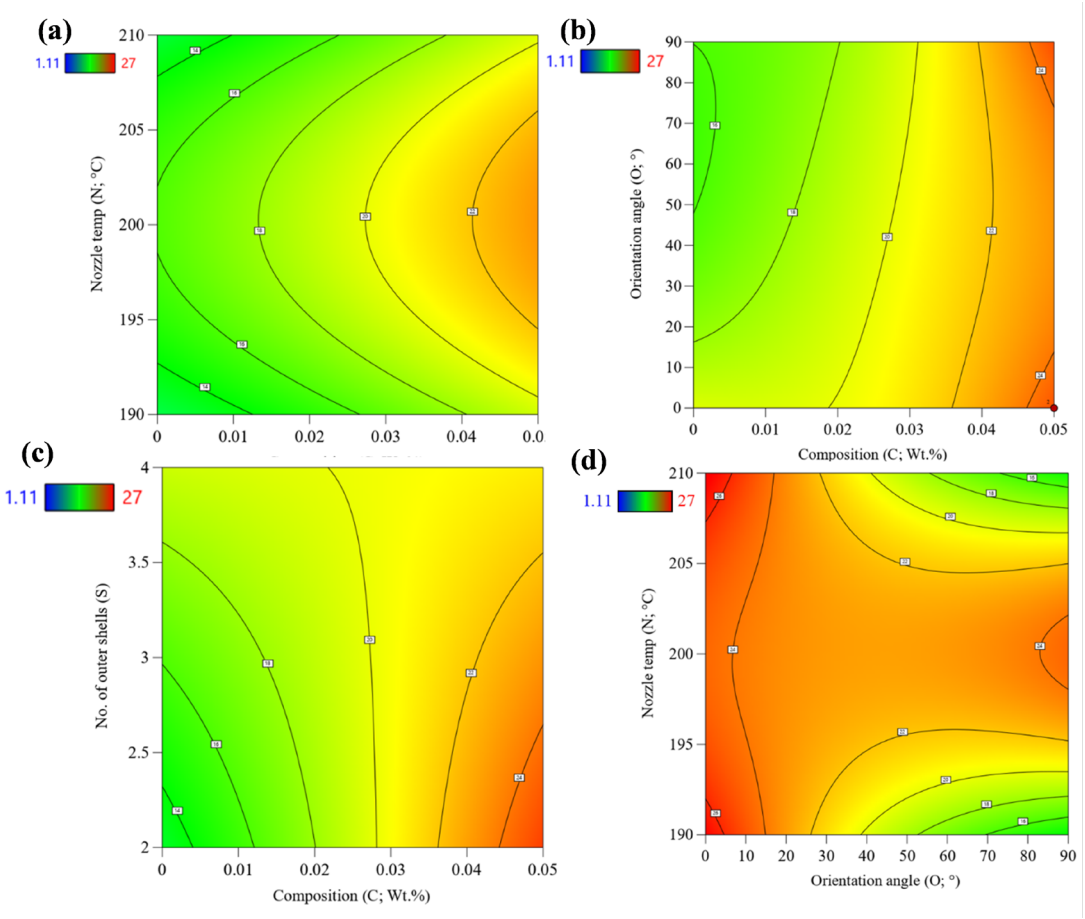


Figure 6. Contour plots for tensile strength. (a) Composition vs. number of outer shells. (b) Composition vs. orientation angle. (c) Composition vs. nozzle temperature. (d) Orientation angle vs. nozzle temperature.

large deviations of up to 25%, increasing dispersion. The results indicate that the tree-based ensemble models generally provide lower prediction errors than MLR for the evaluated responses, with LightGBM showing strong agreement between predicted and experimental values.

The confusion matrices in Figure 10 illustrate the classification performance of machine learning models, namely MLR, AdaBoost, and LightGBM, for tensile strength, Young's modulus, and hardness across four behavioral classes, very low, low, medium, and high, using quartile-based thresholds obtained from the experimental dataset. In Figure 10a–c, tensile strengths below 17.05 MPa were defined as very low, 17.05–20.30 MPa as low, 20.30–22.65 MPa as medium, and values equal to or above 22.65 MPa as high, with accuracies of 67.7%, 61.3%, and 87.1% for MLR, AdaBoost, and LightGBM, respectively, indicating that LightGBM yields the most reliable predictions with the fewest misclassifications. In Figure 10d–f, Young's moduli below 847.00 MPa were defined as very low, 847.00–1,049.80 MPa as low, 1,049.80–1,283.50 MPa as medium, and equal to or above 1,283.50 MPa as high, with accuracies of 41.9% (MLR), 64.5% (AdaBoost), and 77.4% (LightGBM), indicating that MLR exhibits poor performance due to overlap in the classifications, while LightGBM again exhibits superior predictive performance. Similarly, in Figure 10g–i, hardness below 59.3875 HV was defined as very low, 59.3875–65.65 HV as low, 65.65 HV–72.5375 HV as moderate, and equal to or above 72.5375 HV as high, with accuracies of 48.4% (MLR), 61.3% (AdaBoost), and 90.3% (LightGBM). LightGBM achieved excellent classification performance, showing strong diagonal dominance and minimal errors. The results show that, among the three models, LightGBM consistently outperformed across all mechanical properties.

The SHAP analyses in Figure 11 present the relative importance and effects of optimizing printing parameters, including MXene composition, on the predicted responses of MLR (Figure 11a, d, g), AdaBoost (Figure 11b, e, h),

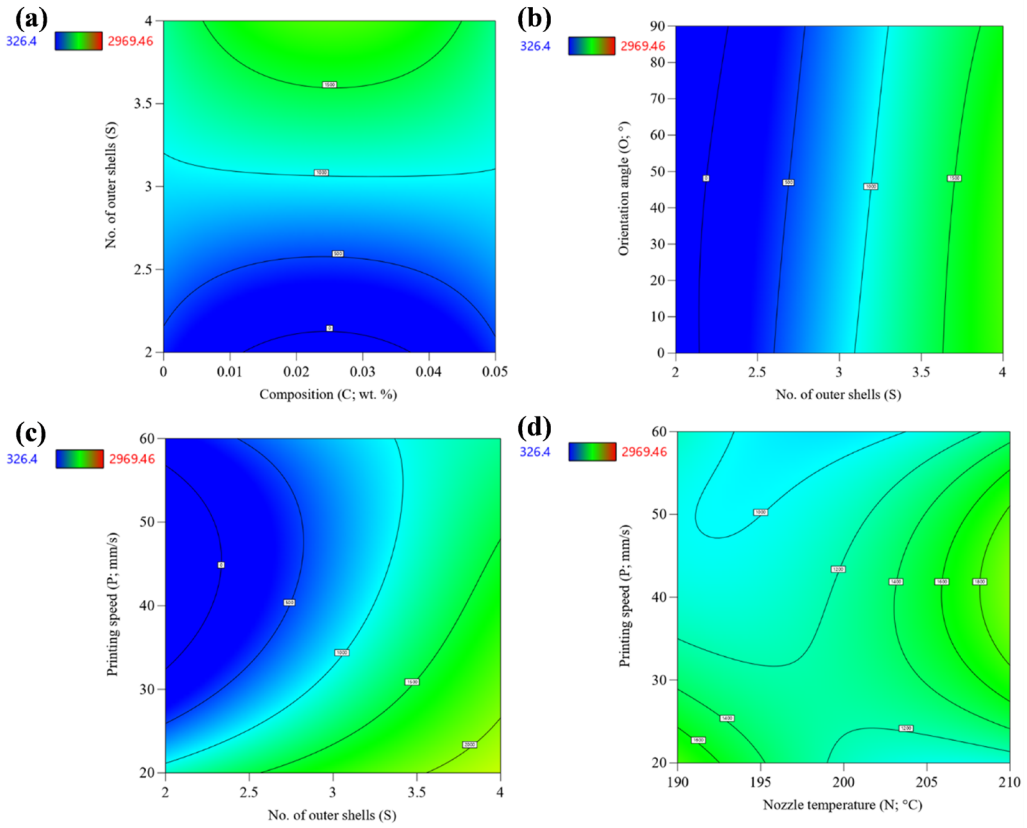


Figure 7. Contour plots of Young's modulus. (a) Composition vs. number of outer shells. (b) Number of outer shells vs. orientation angle. (c) Number of outer shells vs. printing speed. (d) Nozzle temperature vs. printing speed.

and LightGBM (Figure 11c, f, i). For tensile strength (Figure 11a-c), the SHAP value ranged from −10 to 7.5 for LightGBM and from −8 to 6 for AdaBoost, whereas MLR had a narrower range of −1.0 to 0.5, indicating weaker sensitivity. Across all models, orientation angle and composition exhibited the largest SHAP spreads, confirming their dominant influence, whereas printing speed and nozzle temperature showed SHAP values close to zero, indicating minimal contribution. For Young's modulus (Figure 11d–f), the SHAP values were significantly enhanced, with LightGBM and AdaBoost ranging from −600 to 600; meanwhile, MLR was limited to −0.8 to 8.0, indicating poor sensitivity of the linear model. Here, the number of outer shells and nozzle temperature emerged as the most influential parameters. Similarly, for hardness (Figure 11g–i), LightGBM exhibited the widest SHAP distribution (−10 to 10), followed by AdaBoost (−10 to +7.5) and MLR (−0.6 to +0.6). The dominant factors were composition and orientation angle, while nozzle temperature consistently showed near-zero SHAP values across all models. The SHAP distributions provide model-specific information on the magnitude and direction of feature contributions. The tree-based models show broader variation in feature contributions across the dataset, whereas the narrower distributions obtained for MLR are consistent with its linear functional form.

Figure 12 presents the comparative predictive performance of MLR, AdaBoost, and LightGBM for the responses. For tensile strength (Figure 12a), LightGBM was closest to the reference point, showing a very high correlation with the arc lines (R = 0.97–0.99), a standard deviation nearly equal to that of the experimental data, and a minimal RMSE, demonstrating excellent prediction accuracy. Similarly, AdaBoost achieved R of 0.95–0.97 with a slightly higher RMSE, whereas MLR was farther from the reference, indicating weaker correlation and greater deviation. For Young's modulus (Figure 12b), a similar trend was observed, where LightGBM ($R \approx 0.98$) outperformed the other models, followed by AdaBoost (R = 0.95–0.96), and MLR exhibited significant dispersion

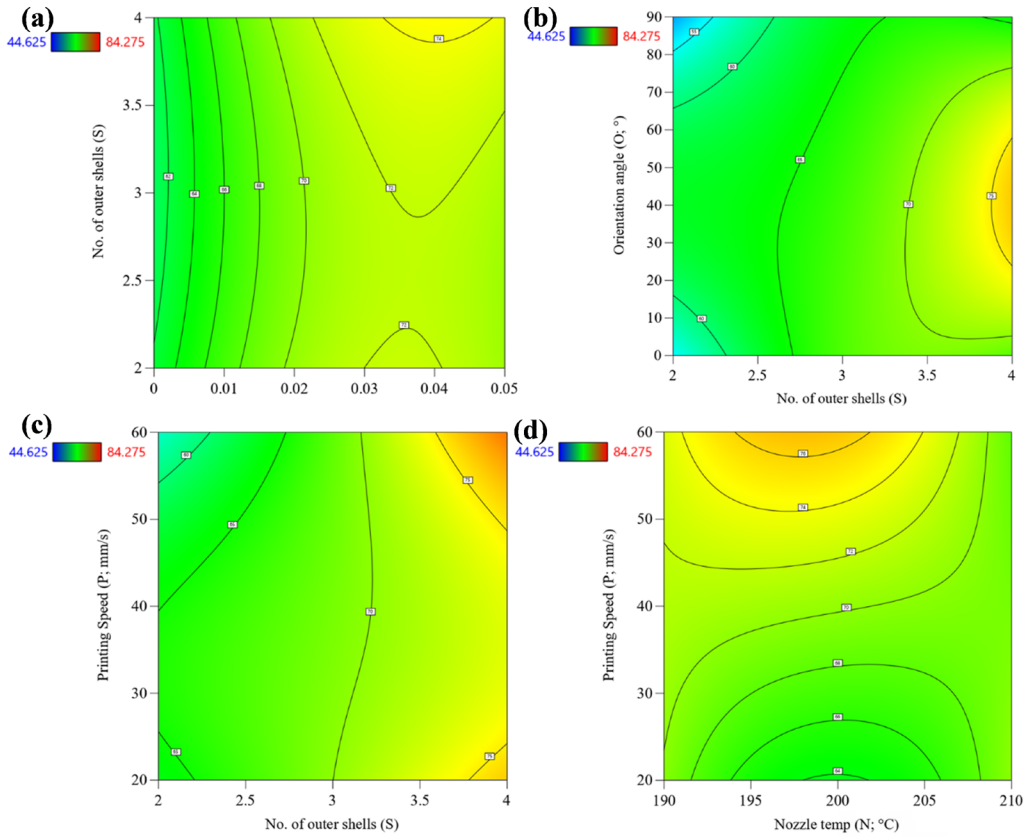


Figure 8. Contour plots of hardness. (a) Composition vs. number of outer shells. (b) Number of outer shells vs. orientation angle. (c) Number of outer shells vs. printing speed. (d) Nozzle temperature vs. printing speed.

and higher error. For hardness (Figure 12c), LightGBM again showed superior performance (R = 0.95–0.96) with the lowest RMSE, followed by AdaBoost (R = 0.90–0.95), while MLR demonstrated poor agreement. Thus, Figure 12 provides a comparative statistical assessment of prediction accuracy, while the subsequent model-interpretation analyses were used to examine the contribution and influence of the input parameters on the predictions.

The Pearson correlation heatmaps (Figure 13) quantify the linear relationships between the printing parameters and the mechanical responses. For tensile strength (Figure 13a), composition (r = 0.56) and number of outer shells (r = 0.31) showed positive correlations, whereas orientation angle (r = −0.59) and printing speed (r = −0.20) showed negative correlations. Nozzle temperature exhibited a weak correlation (r = 0.02). For Young's modulus (Figure 13b), the number of outer shells (r = 0.46) and nozzle temperature (r = 0.38) showed positive correlations, while orientation angle (r = −0.24) and printing speed (r = −0.11) showed negative correlations. Composition showed a weak correlation (r = 0.04). For hardness (Figure 13c), composition (r = 0.37), number of outer shells (r = 0.29), and printing speed (r = 0.29) were positively correlated, whereas orientation angle showed a negative correlation (r = −0.29) and nozzle temperature had a weak correlation (r = −0.04). These results provide a descriptive assessment of linear parameter–response associations and complement the predictive performance analysis. The correlations should not be interpreted as evidence of causation or as a substitute for the multivariable ANOVA and model-interpretation analyses.

For tensile strength (Figure 14a), LightGBM yielded an R^2, MSE, RMSE, MAE, and mean absolute percentage error (MAPE) of 0.96424, 1.11667 MPa², 1.05672 MPa, 0.51183 MPa, and 2.72408%, respectively, compared with 0.93363, 2.07215 MPa², 1.43950 MPa, 1.12779 MPa, and 6.06917% for AdaBoost, and 0.70924, 9.07859 MPa², 3.01307 MPa, 2.36852 MPa, and 34.60431% for MLR. For Young's modulus (Figure 14b), LightGBM again showed superior predictive capability with an R^2 of 0.96491 and

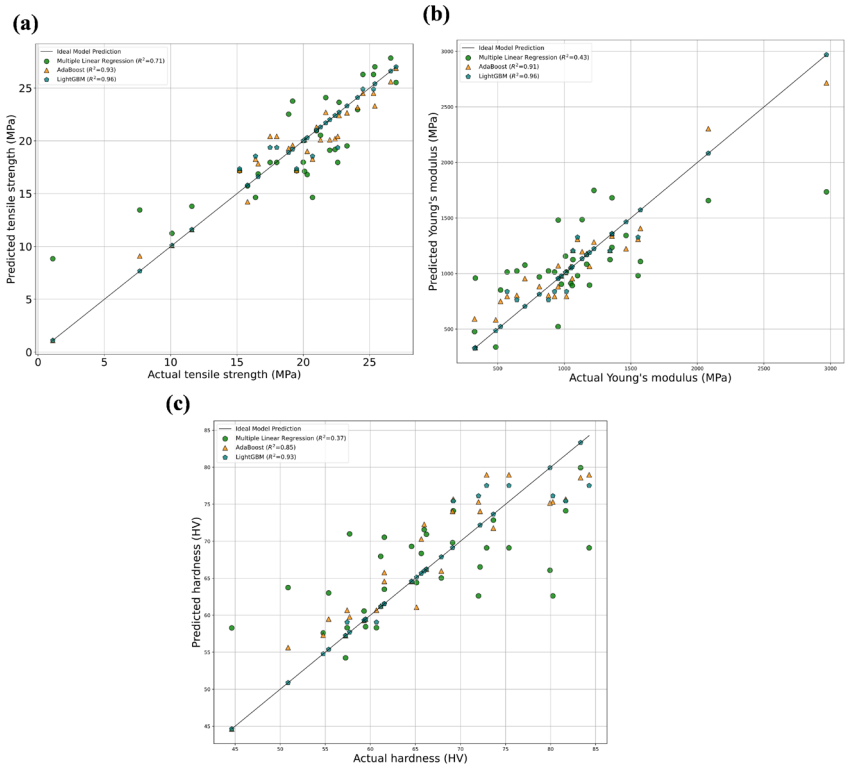


Figure 9. Parity plots comparing different machine learning models with experimental data for (a) tensile strength, (b) Young's modulus, and (c) hardness

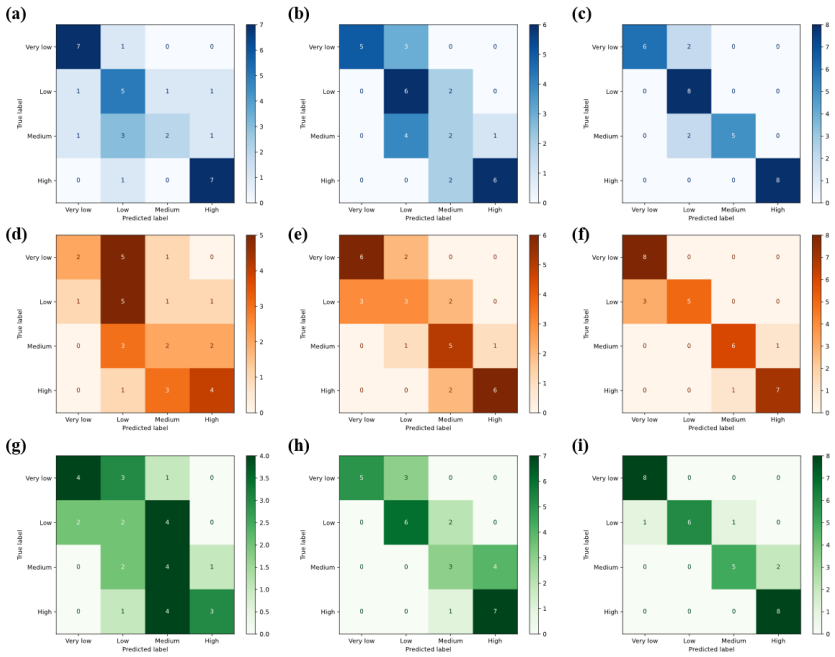


Figure 10. Confusion matrices: (a–c) tensile strength, (d–f) Young's modulus, and (g–i) hardness obtained using multiple linear regression, adaptive boosting, and light gradient boosting machine.

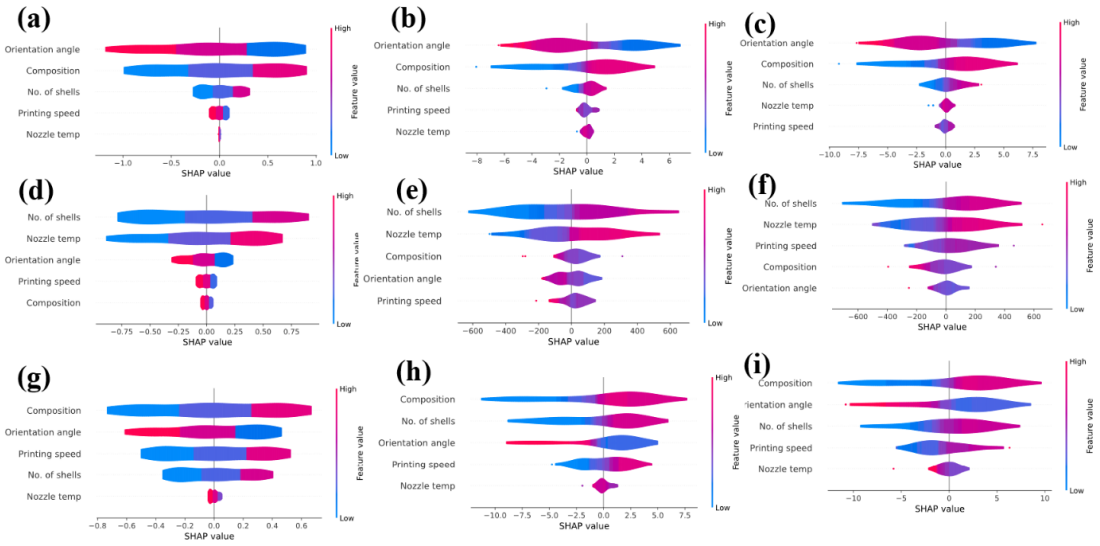


Figure 11. SHapley Additive exPlanations (SHAP) plots illustrating feature contributions to the predictions of (a–c) tensile strength, (d–f)Young's modulus, and (g–i) hardness, obtained using MLR, AdaBoost, and LightGBM, respectively.

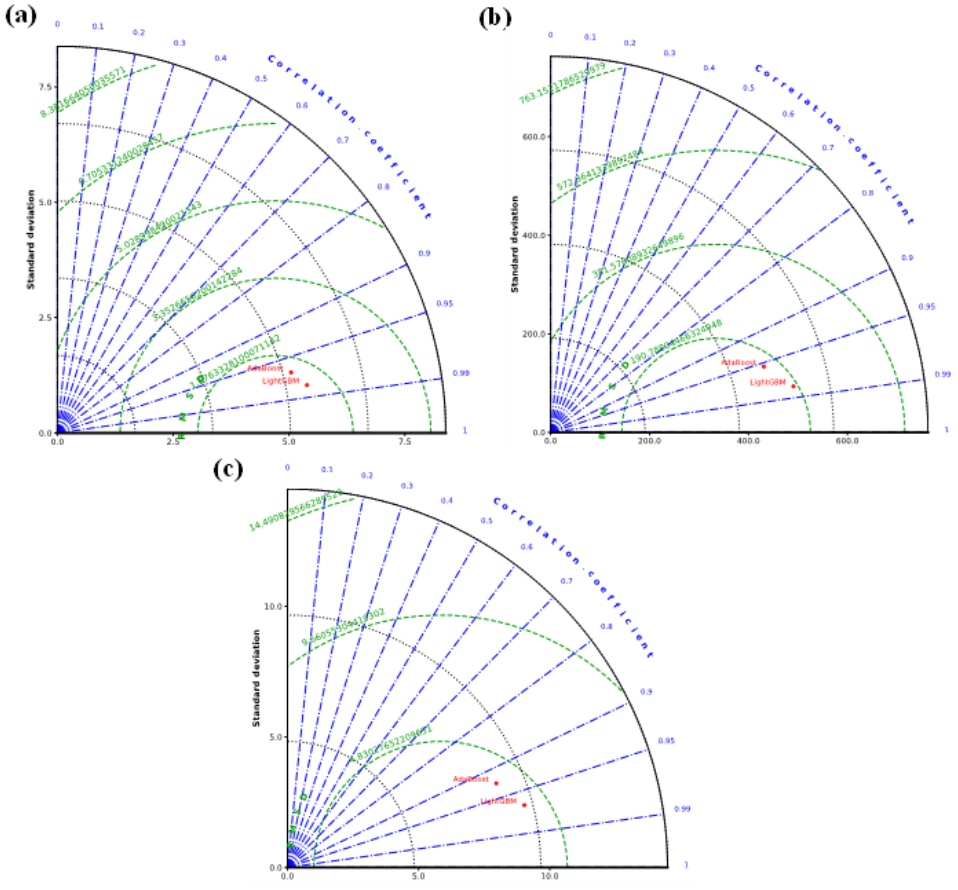


Figure 12. Taylor diagrams for (a) tensile strength, (b) Young's modulus, and (c) hardness across multiple linear regression (MLR), adaptive boosting (AdaBoost), and light gradient boosting machine (LightGBM)

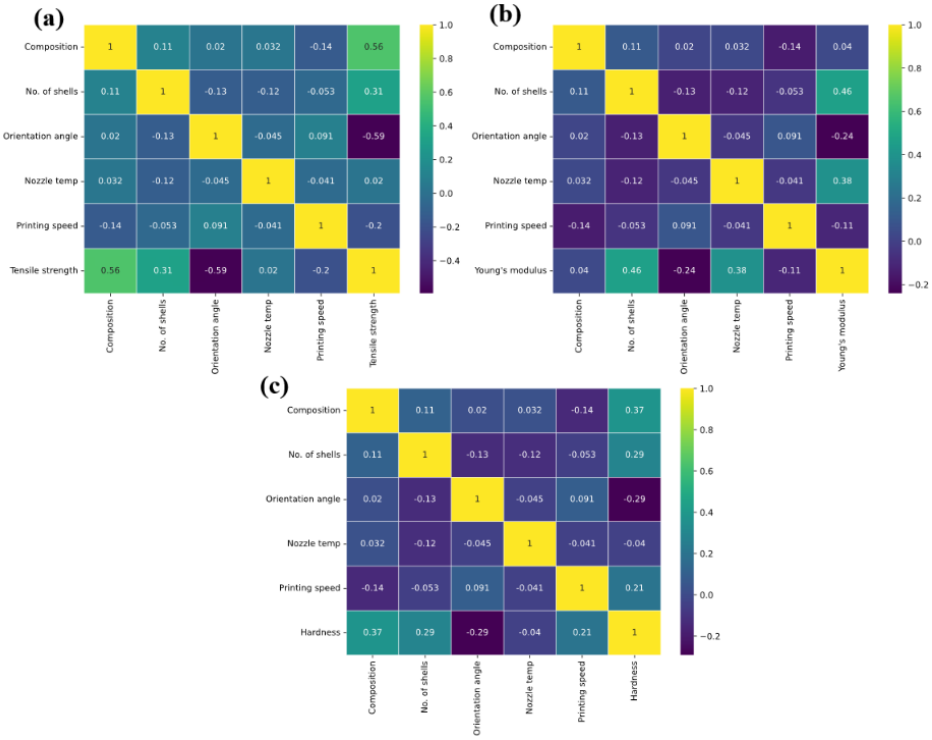


Figure 13. Correlation heatmaps for (a) tensile strength, (b) Young's modulus, and (c) hardness.

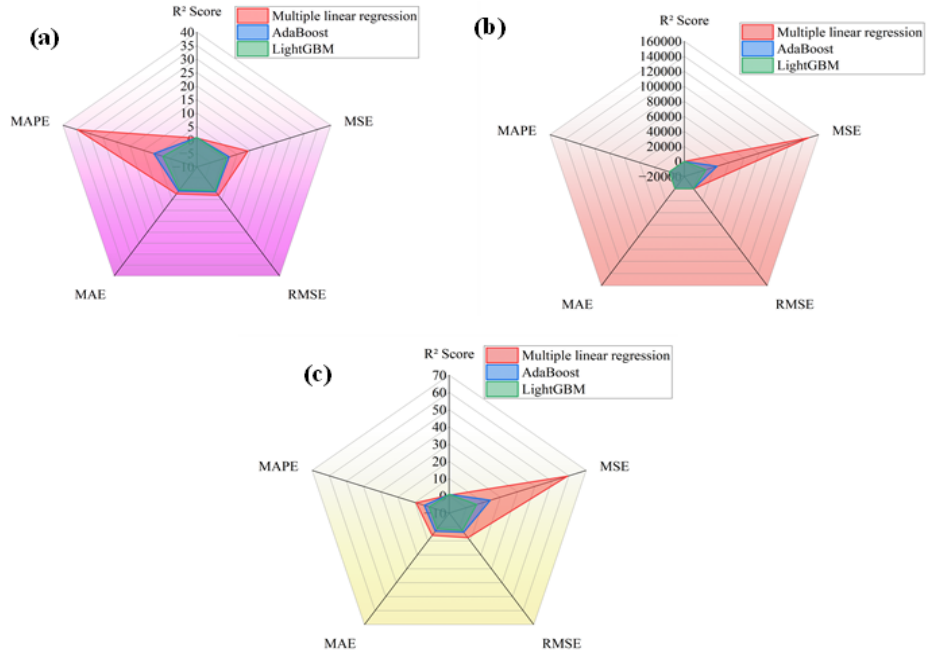


Figure 14. Comparison of predictive performance of machine learning models in (a) tensile strength, (b) Young's modulus, and (c) hardness. Abbreviations: AdaBoost: Adaptive boosting; LightGBM: Light gradient boosting machine; MAE: Mean absolute error; MAPE: Mean absolute percentage error; MSE: Mean squared error; *R*: Coefficient of determination; RMSE: Root mean square error.

markedly lower error values (MSE = 9,083.33599 MPa^2, RMSE = 95.30654 MPa, MAE = 48.56761 MPa, and MAPE = 5.31193%) than AdaBoost and MLR. Similarly, for hardness (Figure 14c), LightGBM achieved the highest R^2 value (0.93478) and the lowest prediction errors (MSE = 6.08712 HV^2, RMSE = 2.46721 HV, MAE = 1.20941 HV, and MAPE = 1.62005%), confirming its superior accuracy over AdaBoost and MLR. The results indicate that LightGBM is the most effective model, followed by AdaBoost, whereas MLR has the weakest predictive performance across all response variables.

3.5. Experimental validation

Figure 15 presents the parity plots comparing the experimental and predicted values obtained using MLR, AdaBoost, and LightGBM for tensile strength, Young's modulus, and hardness. The diagonal line represents ideal agreement, where predicted and experimental values are equal. Points closer to this line indicate better prediction accuracy. For tensile strength, LightGBM achieved good agreement (MAE = 1.866 MPa, RMSE = 2.440 MPa, MAPE = 11.339%, and R^2 = 0.846). For Young's modulus, AdaBoost showed the highest agreement, with an R^2 of 0.905 and an RMSE of 244.665 MPa, compared with 0.586 and 509.802 MPa for MLR and 0.881 and 272.875 MPa for LightGBM. For hardness, AdaBoost achieved an MAE of 2.334 HV, an RMSE of 2.780 HV, a MAPE of 3.598%, and an R^2 of 0.856. The validation results indicate that model performance depends on the response variable: LightGBM provided strong predictions for all three responses, whereas AdaBoost achieved the highest R^2 for Young's modulus and hardness.

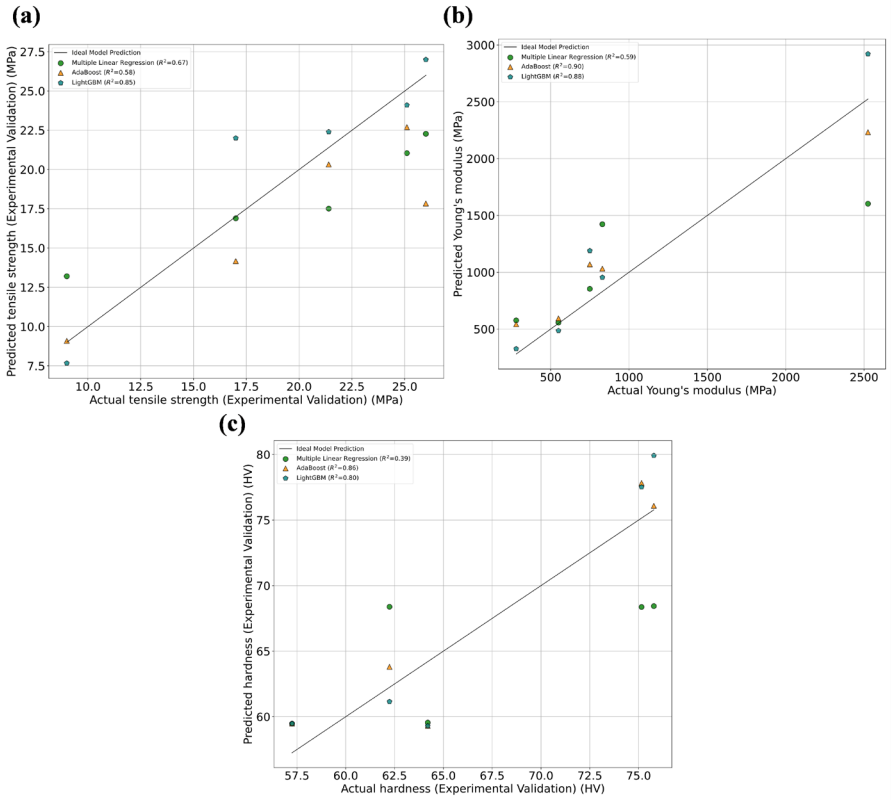


Figure 15. Experimental validation using parity plots of (a) tensile strength, (b) Young's modulus, and (c) hardness
Abbreviations: AdaBoost: Adaptive boosting; LightGBM: Light gradient boosting machine.

4. Conclusion

The study focused on the optimization and prediction of the mechanical properties of MXene-reinforced PLA composites (0–0.05 wt.%) fabricated under varying printing parameters, using RSM–ANOVA and machine learning approaches. The key outcomes are:

- The highest tensile strength reached 27.0 MPa at 0.05 wt.% MXene, 2 outer shells, 0° orientation, 200

°C nozzle temperature, and 20 mm/s printing speed, compared with 22.0 MPa obtained under the selected pure-PLA condition.
- For Young's modulus, outer-shell number and nozzle temperature exhibited the strongest main effects, while orientation angle and printing speed were also statistically significant at the 95% confidence level.
- ANOVA results confirm the statistical significance of the developed models ($R^2 > 0.90$). Composition was the dominant factor influencing tensile strength and hardness, while the number of outer shells and nozzle temperature significantly affected Young's modulus.
- Machine learning models demonstrated strong predictive capability, with LightGBM showing high model-fit performance across the three responses. In the independent experimental validation, LightGBM achieved an R^2 of 0.846 for tensile strength and 0.881 for Young's modulus, while AdaBoost achieved an R^2 of 0.905 for Young's modulus and 0.856 for hardness. These results indicate that predictive performance varied with the response variable.
- SHAP analysis identified composition and printing orientation as influential parameters for tensile strength and hardness, while outer-shell number and nozzle temperature were prominent contributors to Young's modulus.

Acknowledgments

None.

Funding

None.

Conflict of interest

Nitesh Dhar Badgayan is an employee of Ernst and Young Services Private Limited, but was not involved in any activities that could constitute a conflict of interest in relation to this study. The authors declare no competing interests.

Author contributions

Conceptualization: Sundarasetty Harishbabu, Santosh Kumar Sahu

Formal analysis: P. S. Rama Sreekanth, Alagesan Praveen Kumar, Santosh Kumar Sahu, Nitesh Dhar Badgayan, Mohan Kumar Siddalingaiah, Razaullah Hafiz Ullah, Mohammed Aman

Methodology: Sundarasetty Harishbabu, Santosh Kumar Sahu

Writing–original draft: Sundarasetty Harishbabu

Writing–review & editing: P. S. Rama Sreekanth, Alagesan Praveen Kumar, Santosh Kumar Sahu, Nitesh Dhar Badgayan, Mohan Kumar Siddalingaiah, Razaullah Hafiz Ullah, Mohammed Aman

All authors have read and agreed to the published version of the manuscript.

Ethics approval and consent to participate

Not applicable.

Consent for publication

Not applicable.

Availability of data

Data are provided within the manuscript.

References

1. Oladele IO, Oki VO, Omotosho TF, Adebanjo MB, Ayanleye OT, Adekola SA. Sustainable polymer and polymer-based composite materials for extreme conditions and demanding applications—A review on pushing boundaries in materials science. *Next Mater*. 2025;8:100775.

   doi: 10.1016/j.nxmate.2025.100775

2. Rahman MM, Islam S, Mubasshira M, *et al.* Polymer composites in additive manufacturing: Current technologies, applications, and emerging trends. *Polymers.* 2026;18(2):192.

   doi: 10.3390/polym18020192

3. Jha S, Akula B, Enyioma H, Novak M, Amin V, Liang H. Biodegradable biobased polymers: A review of the state of the art, challenges, and future directions. *Polymers.* 2024;16(16):2262.

   doi: 10.3390/polym16162262

4. de Azevedo LC, Rovani S, Santos JJ, *et al.* Biodegradable films derived from corn and potato starch and study of the effect of silicate extracted from sugarcane waste ash. *ACS Appl Polym Mater.* 2020;2(6):2160-2169.

   doi: 10.1021/acsapm.0c00124

5. Arif U, Haider S, Haider A, *et al.* Biocompatible polymers and their potential biomedical applications: A review. *Curr Pharm Des.* 2019;25(34):3608-3619.

   doi: 10.2174/1381612825999191011105148

6. Al-Shalawi FD, Hanim MA, Ariffin MKA, *et al.* Biodegradable synthetic polymer in orthopaedic application: A review. *Mater Today Proc.* 2023;74:540-546.

   doi: 10.1016/j.matpr.2022.12.254

7. Kim KW, Lee BH, Kim HJ, Sriroth K, Dorgan JR. Thermal and mechanical properties of cassava and pineapple flours-filled PLA bio-composites. *J Therm Anal Calorim.* 2012;108(3):1131-1139.

   doi: 10.1007/s10973-011-1350-y

8. Kumar NH, Adarsha H, Keshavamurthy R, Kapilan N. Influence of carbon nano fibre addition on mechanical behaviour of PLA based 3D printed polymer nano composites. *J Inst Eng India Ser D.* 2024;105(1):33-47.

doi: 10.1007/s40033-023-00455-0

9. Bhattacharjee SK, Mondal K, Singh A, *et al.* Impact of nano-silica on thermal, mechanical, and rheological properties of melt-extruded PLA-based nanocomposites. *Int J Biol Macromol.* 2025;321:146077.

doi: 10.1016/j.ijbiomac.2025.146077

10. Triveni BV, Lalithamba HS, Rashmi S, Prashanth GK. Green synthesis of graphitic nanofillers and analysis of 3D-printed graphitic nanofiller-reinforced PLA nanocomposites by impedance spectroscopy. *J Mater Sci Mater Electron.* 2025;36(31):1982.

doi: 10.1007/s10854-025-16025-x

11. Thirugnanasambandam A, Amith SC, Santhosh S, Mukil T, Harsha R, Dharun NK. Mechanical performance of PLA-MWCNT nanocomposite developed by ecofriendly hybrid filament processing method for fused deposition modeling applications. *Polym Compos.* 2025;46(17):15584-15597.

doi: 10.1002/pc.30141

12. Yoon SK, Jang SH, Youk JH, Park NH. Enhanced thermal stability and mechanical properties of PLA nanocomposites reinforced by surface modified halloysite nanotubes. *Polym Eng Sci.* 2026;66(5):3223-3230.

doi: 10.1002/pen.70397

13. Ab Ghani NF, Desa MM, Bijarimi M. The evaluation of mechanical properties graphene nanoplatelets reinforced polylactic acid nanocomposites. *Mater Today Proc.* 2021;42:283-287.

doi: 10.1016/j.matpr.2021.01.501

14. Ramachandran MG, Rajeswari N. Influence of nano silica on mechanical and tribological properties of additive manufactured PLA bio nanocomposite. *Silicon.* 2022;14(2):703-709.

doi: 10.1007/s12633-020-00878-4

15. De Bortoli LS, de Farias R, Mezalira DZ, Schabbach LM, Fredel MC. Functionalized carbon nanotubes for 3D-printed PLA-nanocomposites: Effects on thermal and mechanical properties. *Mater Today Commun.* 2022;31:103402.

doi: 10.1016/j.mtcomm.2022.103402

16. Rong C, Su T, Li Z, *et al.* Elastic properties and tensile strength of 2D Ti3C2Tx MXene monolayers. *Nat Commun.* 2024;15(1):1566.

doi: 10.1038/s41467-024-45657-6

17. Vijayananth K, Palaniappan SK, Singh MK, Pudhupalayam Muthukutti G, Mavinkere Rangappa S, Siengchin S. Exploring MXene-polymer composites for mechanical, tribological, and EMI shielding applications. *Polym Compos.* 2025;46(18):16571-16594.

doi: 10.1002/pc.70084

18. Farahani RD, Dubé M, Therriault D. Three-dimensional printing of multifunctional nanocomposites: manufacturing techniques and applications. *Adv Mater.* 2016;28(28):5794-5821.

doi: 10.1002/adma.201506215

19. Dermanaki Farahani R, Dubé M. Printing polymer nanocomposites and composites in three dimensions. *Adv Eng Mater.* 2018;20(2):1700539.

doi: 10.1002/adem.201700539

20. Karuppusamy M, Thirumalaisamy R, Palanisamy S, Nagamalai S, Massoud EES, Ayrilmis N. A review of machine learning applications in polymer composites: advancements, challenges, and future prospects. *J Mater Chem A.* 2025;13(22):16290-16308.

doi: 10.1039/d5ta00982k

21. Olhan S, Antil B, Maimí P. Machine learning in next-generation polymer composites: Recent advances and perspectives. *Appl Compos Mater.* 2026;33(2):54.

doi: 10.1007/s10443-025-10437-y

22. Chowdary BV, Ali F. Optimisation of surface roughness of FDM fabricated parts: application of definitive screening design and genetic algorithm techniques. *Int J Ind Syst Eng.* 2025;51(2):206-235.

doi: 10.1504/IJISE.2025.148892

23. Srinivasan L, Radhakrishnan L, Veeranan E, Mohammad FK, Moinuddin SQ, Altammar H. NSGA-II-based multi-objective optimization of fused filament fabrication process parameters for TPU parts with chemical smoothing. *Polymers*. 2026;18(3):391.

doi: 10.3390/polym18030391

24. Islam MR, Karim FE, Uddin MB. Optimizing yarn properties through response surface methodology: Finding the ideal flax and cotton fiber proportion in blended yarns by using design-expert software. *SPE Polym.* 2024;5(3):412-425.

doi: 10.1002/pls2.10133

25. Qu DY, Guo FL, Hou WD, Long JF, Li YQ, Fu SY. Cryogenic mechanical properties and liquid oxygen compatibility of MXene/epoxy nanocomposites. *Adv Compos Hybrid Mater.* 2024;7(5):153.

doi: 10.1007/s42114-024-00975-7

26. Hu Y, Liu Y, Cui C, *et al.* Hydroxylated MXene as a nano-binder: Concurrently strengthening interfaces and toughening matrix in carbon fiber/epoxy composites. *Compos Sci Technol.* 2026;273:111426.

doi: 10.1016/j.compscitech.2025.111426

27. Palaniyappan S, Sivakumar NK, Dalaq AS. A peanut-hull-PLA based 3D printing filament with antimicrobial effect. *J Manuf Process.* 2026;160:242-253.

doi: 10.1016/j.jmapro.2026.01.064

28. Kozień D, Malata K, Krysińska Z, *et al.* Fabrication and characterization of PLA-based ceramic composite filaments for FDM 3D printing. *Crystals.* 2026;16(1):46.

doi: 10.3390/cryst16010046

29. Messaoudi R, Mrani I, Majid F. Processing and characterization of PLA/HA composites reinforced with natural sugarcane powder. *BIO Web Conf.* 2026;215:02014.

doi: 10.1051/bioconf/202621502014

30. Liao Y, Liu C, Coppola B, *et al.* Effect of porosity and crystallinity on 3D printed PLA properties. *Polymers.* 2019;11(9):1487.

doi: 10.3390/polym11091487

31. Sapre M, Jatti AV, Khedkar NK, Jatti VS. Mechanical properties of 3D-printed components using fused deposition modeling: Optimization using the desirability approach and machine learning regressor. *Appl Syst Innov.* 2022;5(6):112.

doi: 10.3390/asi5060112

32. Sahu SK, Sreekanth PSR. Artificial neural network for prediction of mechanical properties of HDPE based nanodiamond nanocomposite. *Polym Korea.* 2022;46(5):614-620.

doi: 10.7317/pk.2022.46.5.614

33. Ghorbal GB, Tricoteaux A, Thuault A, Louis G, Chicot D. Comparison of conventional Knoop and Vickers hardness of ceramic materials. *J Eur Ceram Soc.* 2017;37(6):2531-2535.

doi: 10.1016/j.jeurceramsoc.2017.02.014

34. Gaesenngwe G, Danha G, Raghupatruni PVS, Mamvura TA. The significance of coal ball milling model equations in manufacturing industries. *Int J Coal Prep Util.* Published online January 8, 2026.

doi: 10.1080/19392699.2025.2605273

35. Boudboud A, Ben Aziz M, Arif S, *et al.* Optimizing polyphenol oxidases activity of apricot fruits using Box-Behnken design and evaluation of their inhibition by thermal, chemical, and plant extracts treatment. *J Food Meas Charact.* 2026;20(8):6109-6123.

doi: 10.1007/s11694-026-04054-x

36. Sundarasetty H, Sahu SK. Tribological behavior of PLA reinforced with boron nitride nanoparticles using Taguchi and machine learning approaches. *Results Eng.* 2025;26:104772.

doi: 10.1016/j.rineng.2025.104772

37. Louhichi B, Joy D, Sahu SK, *et al.* Methods to optimize tribological properties of pineapple leaf fiber epoxy composites. *Ind Crops Prod.* 2026;242:122865.

doi: 10.1016/j.indcrop.2026.122865

38. Rahmani S, Belkadi AA, Achour Y, *et al.* Machine learning models with SHAP for performance prediction of eco-friendly fiber reinforced mortars with glass waste. *Sci Rep*. 2025;15(1):40973.

doi: 10.1038/s41598-025-24781-3

39. Harishbabu S, Alrasheedi NH, Louhichi B, Sahu SK, Ma Q. Optimization and prediction of mechanical properties of additively manufactured PLA/GNP composites via response surface methodology and machine learning models. *Polymers.* 2025;17(21):2894.

doi: 10.3390/polym17212894

40. Schapire RE. Explaining AdaBoost. In: Schölkopf B, Luo Z, Vovk V, eds. *Empirical Inference*. Springer; 2013:37-52.

doi: 10.1007/978-3-642-41136-6_5

41. Rufo DD, Debelee TG, Ibenthal A, Negera WG. Diagnosis of diabetes mellitus using gradient boosting machine (LightGBM). *Diagnostics.* 2021;11(9):1714.

doi: 10.3390/diagnostics11091714

42. Guo J, Yun S, Meng Y, *et al.* Prediction of heating and cooling loads based on light gradient boosting machine algorithms. *Build Environ.* 2023;236:110252.

doi: 10.1016/j.buildenv.2023.110252